Macromolecules

pubs.acs.org/Macromolecules Article

Concentration and Temperature Dependence of the Interaction Parameter and Correlation Length for Poly(benzyl methacrylate) in Ionic Liquids

Brian R. Carrick, Steven Weigand, Claire L. Seitzinger, and Timothy P. Lodge*

Cite This: https://doi.org/10.1021/acs.macromol.2c01365 Read Online

ACCESS | Metrics & More | Article Recommendations | Supporting Information

ABSTRACT: Polymers in ionic liquids (ILs) are a fascinating class of materials which exhibit unusual behavior in comparison to more traditional polymer solutions. Previous work characterizing the lower critical solution temperature (LCST) phase behavior of poly(benzyl methacrylate) (PBnMA)/IL mixtures demonstrated that the second virial coefficient is consistently positive, even at temperatures above the observed phase separation boundary and that the critical composition is shifted strongly toward polymer-rich compositions. To better understand these phenomena, small-angle X-ray scattering was utilized along with the random phase approximation to determine the interaction parameter and correlation length of PBnMA in four ILs (one pyrrolidinium-based and three imidazolium-based) as a function of temperature (25−170 °C), concentration (5−30 wt %), and molecular weight (32−76 kDa). The interaction parameter was shown to increase with polymer volume fraction, contrary to the concentration-independent behavior anticipated by Flory-Huggins theory, which clarified the unusual phase diagram of these solutions. The semidilute correlation length of PBnMA in 1-butyl-1-methylpyrrolidinium bis(trifluoromethylsulfonyl)imide was shown to obey a temperature-concentration master curve; however, no such universal behavior was exhibited among the four ILs. Additionally, the concentration dependence of the correlation length was shown to decrease as the solvent quality worsened.

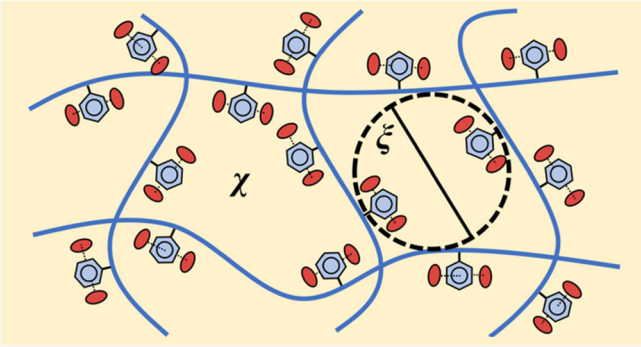

■ INTRODUCTION

Polymers in ionic liquids (ILs) are a growing class of materials of interest for use in wide ranging applications, including battery electrolytes, separation membranes, and electrochemical devices.[1−4] The polymer provides mechanical strength while maintaining the IL diffusivity and ionic conductivity.[5] Incorporating stimuli-responsive behavior into these systems could further expand their applications in sensing, smart coatings, and actuators.[6] However, their scope is currently constrained as a plethora of fundamental questions surrounding these behaviors remain unanswered.

A thermo-responsive system of interest is poly(benzyl methacrylate) (PBnMA), which exhibits lower critical solution temperature (LCST) phase behavior in multiple ILs.[7] This unusual behavior was first demonstrated by Watanabe and co-workers, who hypothesized that IL clathrates solvate the polymer at room temperature but dissipate during phase separation upon heating.[8] Additionally, through a combination of X-ray scattering and all-atom molecular dynamics simulations, it has been shown that PBnMA exhibits intramolecular $\pi-\pi$ stacking between adjacent benzyl groups, causing the polymers to exist in relatively compact conformations at room temperature, rather than as swollen chains as is typically observed in good solvents.[9] This latter conclusion, however, is not consistent with the extensive dynamic light scattering results of Kharel et al., which showed swollen chain conformations.[10] Recent work from our group has demonstrated that the second virial coefficient of PBnMA in dilute IL solutions is consistently positive, even above temperatures where phase separation is observed at higher concentrations and that the critical compositions of the phase diagrams are strongly displaced toward polymer-rich concentrations.[10,11] These observations deviate from the behavior anticipated by Flory−Huggins theory and observed in many other LCST systems; they may reflect a strongly concentration-dependent interaction parameter. These phenomena pose foundational questions about the solvation of PBnMA in ILs, which we explore here.

Received: July 1, 2022
Revised: September 5, 2022

It was first proposed by de Gennes that the structure factor for polymer blends and concentrated solutions follows a random phase approximation (RPA).[12] This mean-field approach allows for the interaction parameter (χ) at a specific concentration to be determined through small-angle X-ray scattering (SAXS) or small-angle neutron scattering (SANS), whereas light scattering is only able to obtain χ in dilute solutions. Previous studies have applied the RPA to determine χ for numerous polymer blends and solutions.[13−18] According to the mean-field approach, the Ornstein−Zernike equation can also be used to assess the correlation length (ξ), or the average distance between overlapping chain segments, beyond which chains no longer experience excluded volume effects from adjacent segments.[19]

This work focuses on a comprehensive examination of χ and ξ for PBnMA in one pyrrolidinium-based and three imidazolium-based ILs over a wide range of concentrations, molecular weights, and temperatures, via small-angle X-ray scattering. The use of ILs offer unprecedented control over the solvent quality by varying the temperature or cation identity; this feature is exploited to probe the solution behavior. Additionally, approximate spinodal curves were constructed from Ornstein−Zernike analysis and discussed with respect to a concentration-dependent interaction parameter and possible local ordering of the IL.

■ MATERIALS AND METHODS

Polymer Characterization. PBnMA was synthesized previously via atom transfer radical polymerization.[10,11] The polymers under study are denoted PBnMA-x, where x represents the polymer weight-average molecular weight in kDa. The number-average molecular weight (M_n), weight-average molecular weight (M_w), and dispersity ($Đ$) of the polymers are summarized in Table 1 as determined by size exclusion chromatography performed in THF on an Agilent 1260 Infinity System (Agilent Technologies, Santa Clara, CA, USA). The eluent was monitored using a Wyatt Optilab T-rEX (Wyatt Technology, Santa Barbara, CA, USA) refractive index detector (Figure S1) and a Wyatt Dawn Heleos II multiangle laser light scattering detector. The dn/dc of PBnMA in THF is 0.144 mL/g.[20] A representative ^{1}H NMR spectrum of PBnMA-76 in CD_2Cl_2 is shown in Figure S2, as collected on a Bruker Avance III HD nanobay AX-400 spectrometer (Bruker, Billerica, MA, USA) with a shielded Ascend magnet and a SampleXpress autosampler.

Table 1. Characteristics of PBnMA As Determined via SEC-MALS in THF

sample	M_n (kDa)	M_w (kDa)	$Đ$
PBnMA-32	27	32	1.19
PBnMA-63	55	63	1.15
PBnMA-76	64	76	1.19

Solution Preparation. The ionic liquids 1-butyl-1-methylpyrrolidinium bis(trifluoromethyl-sulfonyl)imide ([BMP][TFSI]) and 1,3-dimethylimidazolium TFSI ([MMIM][TFSI]) were purchased from IoLiTec GmbH (Heilbronn, Germany) and dried under vacuum for 48 h prior to use. 1-Ethyl-3-methylimidazolium TFSI ([EMIM][TFSI]) and 1-butyl-3-methyl-imidazolium TFSI ([BMIM][TFSI]) were synthesized via ion exchange in water as previously reported and dried under vacuum prior to use.[21] Representative ^{1}H and ^{19}F NMR spectra of the ionic liquids in DMSO-d_6 are shown in Figures S3−S6. Solutions were prepared via co-solvent evaporation at concentrations above the overlap concentration, c^*. Additionally, the concentration in wt% was converted to g/mL and volume fraction by assuming no volume change upon mixing. The density of each ionic liquid (ρ) was estimated from $\rho = b - aT$, where a and b are parameters collected in Table S1, and the density of PBnMA was taken to be constant at 1.18 g/cm^3.[22−24]

Rheology. The overlap concentration c^* for PBnMA in [BMP][TFSI] was estimated according to steady-shear rheology performed on a TA Instruments Discovery HR3 Rheometer (Texas Instruments, Dallas, TX, USA) equipped with 40 mm stainless steel plates, where the upper plate is electronically heated. Temperature sweeps from 25−180 °C were performed with a gap thickness of ∼300 μm, a shear rate of 1.0 s^{-1}, and a heating rate of 1 °C/min for concentrations from 5−25 wt % PBnMA-32, as shown in Figure S7. The overlap concentration was approximated as the concentration at which the solution viscosity is twice that of the pure solvent.[22,25] The 5 wt % PBnMA-32 solution was shown to follow this constraint over the entire temperature range; therefore, all solutions were prepared at or above 5 wt % PBnMA, and all have $c \geq c^*$.

Small-Angle X-ray Scattering. Small-angle X-ray scattering (SAXS) measurements were performed at the 5-ID-D beamline of the Dupont-Northwestern-Dow Collaborative Access Team (DND-CAT) at the Advanced Photon Source, Argonne National Laboratory. Solutions were charged into 1.5 mm diameter quartz capillaries and sealed with epoxy. [BMP][TFSI] solutions were placed into an 8-capillary temperature-controlled heating stage and were heated to 25, 60, 90, 110, 130, 150, and 170 °C at 10 °C/min and annealed at each temperature for 5 min prior to taking measurements. Solutions of imidazolium-based ILs were placed into a 29-capillary holder and measured at ambient temperature. Two-dimensional scattering patterns were collected for 1 s exposure times to X-rays at λ_o = 0.7293 Å with a Rayonix MX170-HS CCD area detector at a sample-to-detector distance of 8.5 m. The scattering vector ($q = (4\pi/\lambda)\sin(\theta/2)$, where λ is the beam wavelength in the material and θ is the scattering angle) ranged from q = 0.002−0.192 Å^{-1}. The observed intensity was normalized against a glassy carbon standard, yielding the absolute intensity (I). One-dimension scattering patterns of the form $I(q)$ vs q were obtained by azimuthally averaging the isotropic two-dimensional data. Finally, the background (pure IL and capillary scattering) was fit to a power-law ($I(q) = Aq^{-P} + B$) and subtracted from the solution scattering at each temperature. Scattering patterns of the pure ILs at each temperature are collected in Figure S8 alongside their corresponding power-law fits. It should be noted that this method of background subtraction results in a low-q upturn, which is indicative of incomplete background subtraction of the capillary, pure IL, and sample environment. However, this is typical of solution SAXS in capillaries and leads to no discernible difference in the data for q > 0.02 Å^{-1} nor in the resulting fit parameters, than if the low-q upturn was subtracted via a power-law fitting of the individual solution low-q scattering.

Wide-angle X-ray scattering (WAXS) data were simultaneously collected with a Rayonix LX170-HS CCD area detector at a sample-to-detector distance of 200 mm over a q range of 0.68−4.46 Å^{-1}. The observed intensity was normalized against a glassy carbon standard, yielding the absolute intensity. Two-dimensional isotropic scattering patterns were azimuthally averaged to yield one-dimensional plots of $I(q)$ vs q; no background subtraction was performed.

■ RESULTS

SAXS measurements were performed for each polymer in [BMP][TFSI] over concentrations and temperatures ranging from 5−30 wt % and 25−170 °C. Representative scattering patterns for PBnMA in [BMP][TFSI] are shown in Figure 1a,c; plots for the remaining [BMP][TFSI] solutions are located within Figures S9−S14. Additionally, profiles of PBnMA-32 and PBnMA-76 in [MMIM][TFSI], [EMIM][TFSI], and [BMIM][TFSI] were collected at 25 °C for 10−20 wt % and are reported in Figure S15. Upon crossing the cloud point temperature (T_{CP}), as determined from previous work, solutions undergo phase separation into polymer-rich and solvent-rich phases.[11] As such, measurements above T_{CP}

https://doi.org/10.1021/acs.macromol.2c01365
Macromolecules XXXX, XXX, XXX−XXX

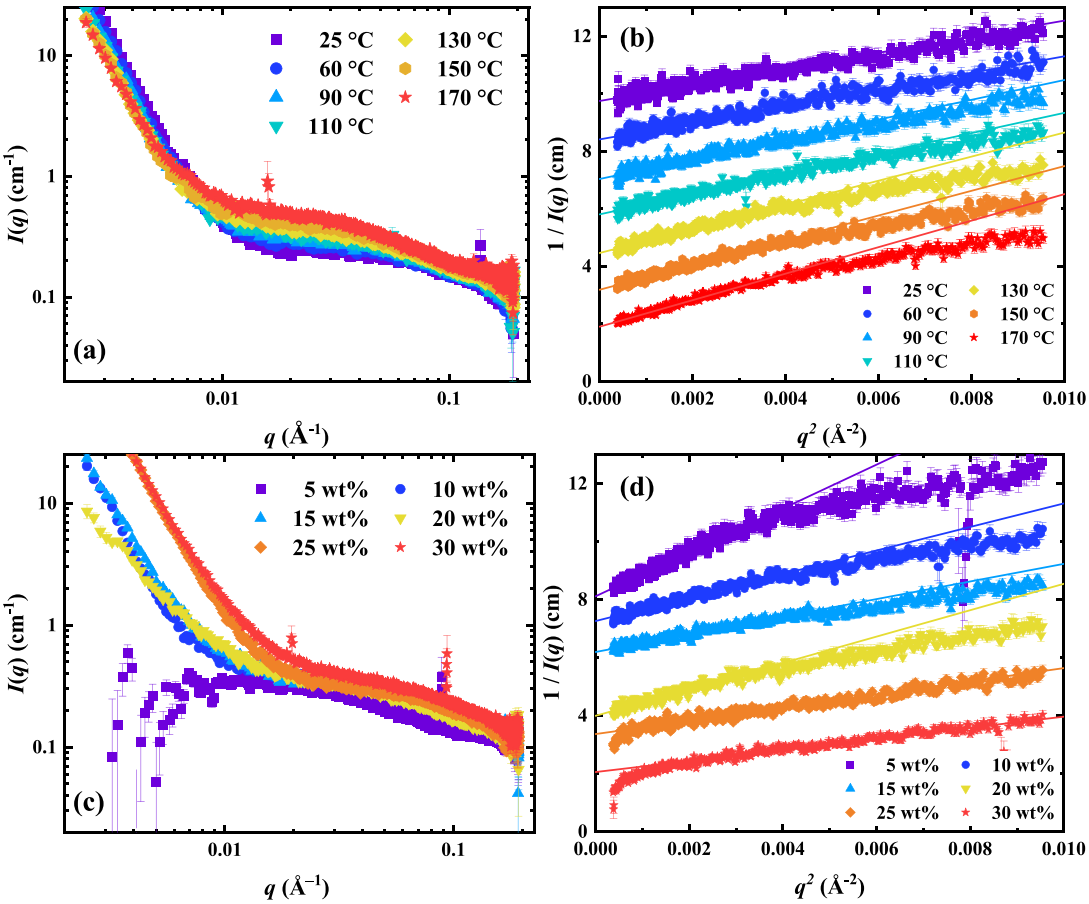

Figure 1. Representative SAXS intensity scattering profiles of (a) 10 wt % PBnMA-63 at various temperatures and (c) PBnMA-63 for several concentrations at 130 °C. Ornstein−Zernike plots for (b) 10 wt % PBnMA-63 in [BMP][TFSI] at several temperatures with best fit lines and (d) PBnMA-63 for various concentrations at 130 °C; data have been truncated and vertically shifted.

are out of equilibrium and are not considered in the subsequent analysis.

The scattering intensity of entangled polymer solutions arises from local concentration fluctuations as the chain segments relax under thermal motion. For an LCST system such as PBnMA in [BMP][TFSI], these fluctuations increase with temperature as the solutions approach their phase boundaries. Following background subtraction, the scattering pattern is anticipated to plateau at low-q and then exhibit standard OZ behavior at high-q, where the intensity decreases proportionally to q^{-2}. However, there are two characteristic features in the scattering patterns in Figure 1a,c beyond those typically observed in polymer solutions. The first feature is excess scattering at low-q, which is an artifact of improper background subtraction in solution SAXS in capillaries. The second unique feature is more readily observed in the scattering patterns of the neat ILs (Figure S8), where there is a small uprun at high-q due to local ordering of the IL.[26]

The scattering profiles were according to the Ornstein−Zernike (OZ) equation (eq 1), as illustrated in Figure 1b,d, for PBnMA-63 in [BMP][TFSI]:[19]

$$I(q) = \frac{I(0)}{1 + (q\xi)^2} \tag{1}$$

where $I(0)$ is the intensity at zero scattering angle and ξ is the correlation length.[19] Additional OZ plots are collected in Figures S16−S19. The initial linear regime at low q^2 was fit to obtain $I(0)$ and ξ; this linear regime decreases in size as the temperature increases, as shown in Figure 1b.

The RPA has long been used to evaluate the scattering of polymer blends and solutions:[19]

$$\frac{(\Delta\mathrm{SLD})^2}{I(q)} = \frac{1}{\Phi_P \hat{V}_P P(q)} + \frac{1}{\Phi_{IL} \hat{V}_{IL}} - \frac{2\chi}{\hat{V}_{IL}} \tag{2}$$

where ΔSLD is the difference in scattering length density between PBnMA and the IL, Φ_P and Φ_{IL} are the volume fractions of PBnMA and the IL, and $\hat{V}_P$ and $\hat{V}_{IL}$ are the corresponding molar volumes. The molar volume and scattering length density of each component were calculated at every temperature to account for the temperature dependence of the IL density by $\hat{V}_i = M_{w,i}/\rho_i$ and $\mathrm{SLD}_i = (N_{av}/\hat{V}_i)\sum b_{c,i}$, respectively, where N_{av} is Avogadro's number and $\sum b_c$ is the sum of the scattering length of all atoms in a molecule. The form factor of the polymer chains, $P(q)$, was approximated by the Debye function:[19]

$$P(q) = \frac{2}{q^4 R_g^4}[\exp(-q^2 R_g^2) - 1 + q^2 R_g^2] \tag{3}$$

where R_g is the radius of gyration. The RPA relies upon the following assumptions: (1) there are many overlapping polymer chains in solution, (2) chains can fully relax their conformations, and (3) they adopt Gaussian conformations. As such, it is important that the solutions are above the overlap concentration c^*, which was determined to be approximately 5

https://doi.org/10.1021/acs.macromol.2c01365
Macromolecules XXXX, XXX, XXX−XXX

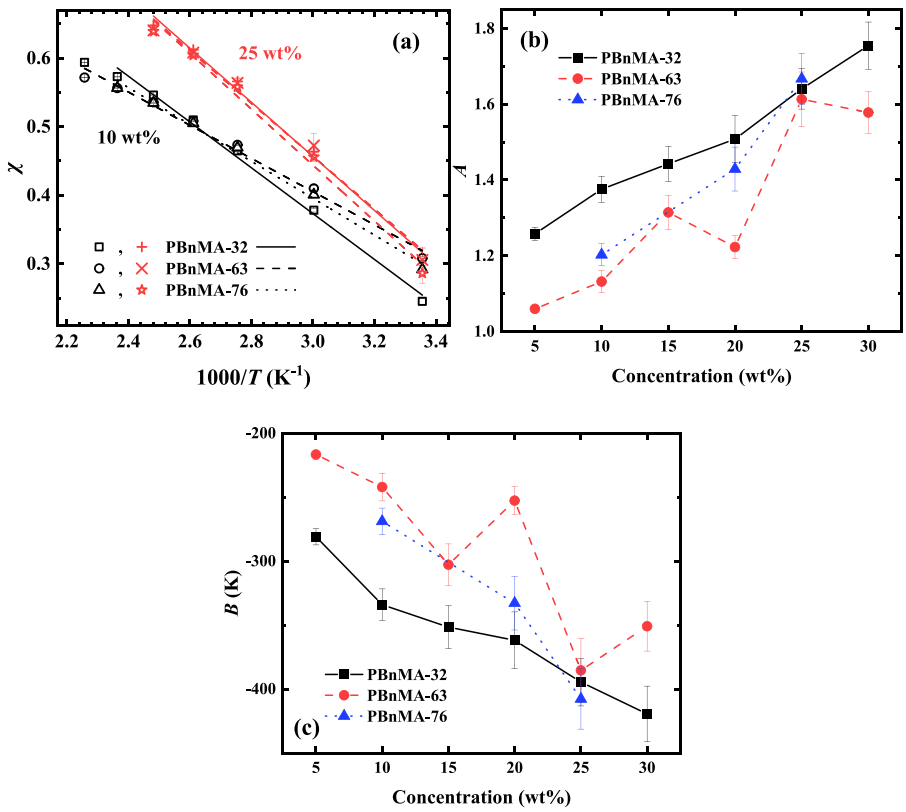

Figure 2. (a) Reciprocal temperature dependence of χ as determined from the RPA at 10 and 25 wt % PBnMA in [BMP][TFSI] for each molecular weight. The lines are linear fits. (b) Excess entropic, A, and (c) enthalpic, B, components of χ as a function of polymer concentration for PBnMA in [BMP][TFSI] for each molecular weight. The lines serve as the guide to the eye.

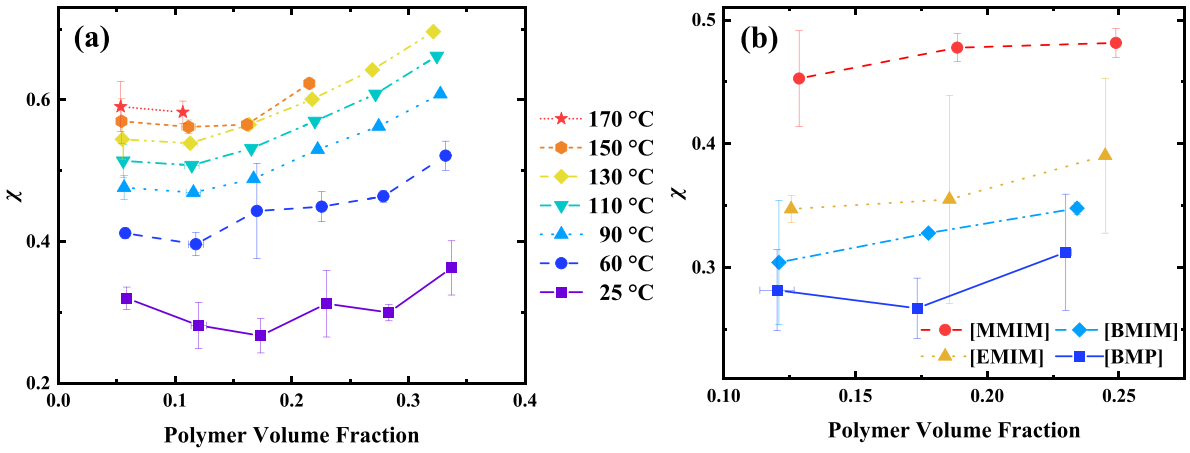

Figure 3. Concentration dependence of χ averaged across all molecular weights as determined from the RPA for PBnMA in (a) [BMP][TFSI] at various temperatures and in (b) various ILs at 25 °C. The lines serve as the guide to the eye.

wt % in [BMP][TFSI] for the lowest molecular weight polymer, PBnMA-32, as the solution viscosity was twice that of pure solvent throughout the entire temperature range under study.[25]

In the zero-angle limit, the RPA can be expressed as follows:

$$\frac{(\Delta \mathrm{SLD})^2}{I(0)} = \frac{1}{\Phi_P \hat{V}_P} + \frac{1}{\Phi_{IL} \hat{V}_{IL}} - \frac{2\chi}{\hat{V}_{IL}} \tag{4}$$

This allows for facile conversion of the $I(0)$ obtained from the OZ equation to determine χ for an individual solution. It should be noted that scattering patterns could instead be fit to the RPA (eq 2) over a wide-range of q to obtain χ. While the trends with respect to temperature, concentration, and molecular weight remain qualitatively similar via this approach, it tends to give systematically lower values of χ. Additionally, the use of the OZ form emphasizes the q range where one would typically examine to extract thermodynamic parameters in polymer solutions. In practice, the extracted χ is inversely related to temperature according to $\chi = A + B/T$, where A encompasses the excess entropic contributions and B encompasses the enthalpic contributions. The reciprocal temperature dependence of χ for 10 and 25 wt % PBnMA in [BMP][TFSI] is shown in Figure 2a, and the χ of other

https://doi.org/10.1021/acs.macromol.2c01365
Macromolecules XXXX, XXX, XXX−XXX

[BMP][TFSI] solutions are collected in Figure S20. The values of A and B at a specific concentration and molecular weight were determined according to the lines of best fit of the reciprocal temperature dependence of χ and are collected in Figure 2b,c, respectively. The magnitude of both parameters monotonically increases by ~1.5 and ~1.6 times the original value for A and B, respectively, as the concentration increases from 5 to 30 wt %. Molecular weight is observed to have a minor-to-negligible influence on χ, A, and B.

The interaction parameters for PBnMA in ILs are collected and plotted in Figure S21 as a function of polymer volume fraction for each temperature and molecular weight. Because χ is independent of molecular weight, it was averaged at each composition and temperature, and the resulting χ are shown in Figure 3a,b for [BMP][TFS] and the imidazolium-based ILs, respectively. For each IL, χ increases with polymer volume fraction. Additionally, χ increases as the solvent quality worsens, as demonstrated by increasing the temperature of [BMP][TFSI] solutions or varying the cation identity from [BMP] to [MMIM]. These trends agree with light scattering results of Kharel et al. and with cloud point measurements of Ueki et al.[10,27]

Additionally, the spinodal curves for PBnMA in [BMP][TFSI] solutions can be estimated according to the temperature dependence of the zero-angle scattering intensity. As shown in Figure 1b, $1/I(q)$ decreases as samples are heated and approach phase separation. By plotting $1/I(0)$ as a function of $1/T$, the spinodal temperatures (T_S) can be estimated via extrapolation to infinite zero-angle scattering intensity ($1/I(0) = 0$) for temperatures within the vicinity of phase separation; the plots and the corresponding extrapolations for PBnMA solutions in [BMP][TFSI] are collected, as shown in Figure S22. The nonlinearity of $1/I(0)$ vs $1/T$ at low temperatures and the large extrapolation distance make the determination of T_S relatively uncertain, but the fitting was performed on data points exhibiting a linear response near phase separation. These deviations may arise because the compositions lie far from the critical composition or because the temperatures are much lower than the spinodal temperature, leading to weak concentration fluctuations. This is indicated by observing the largest deviations at lower temperatures and concentrations, which are farthest from the spinodal curve and critical composition, respectively. Nevertheless, the spinodal temperatures from these extrapolations are compiled to construct the approximate phase diagrams shown in Figure 4, alongside previously measured cloud point curves.[11] T_S decreases with concentration beyond the anticipated critical concentration (*ca.* 6−9 wt %), similar to the previously measured binodal curves. However, the gap between the spinodal and coexistence curves is large (*ca.* 150 °C at 30 wt %), also suggesting that the critical composition lies at even higher concentrations than explored here.

Solutions with polymer concentrations above c^* exhibit a unique length scale that describes the average distance between overlapping segments, the correlation length (ξ), or the blob size, which can be determined using the OZ form (eq 1).[12] The temperature dependence of the correlation length of PBnMA in [BMP][TFSI] is shown in Figure S23. As the temperature increases and solutions approach phase separation, the correlation length increases, however, a weaker temperature dependence is observed at lower concentrations. For example, the 5 and 20 wt % PBnMA-32 solutions in [BMP][TFSI] exhibit approximately a 2 and 6 Å increase in ξ

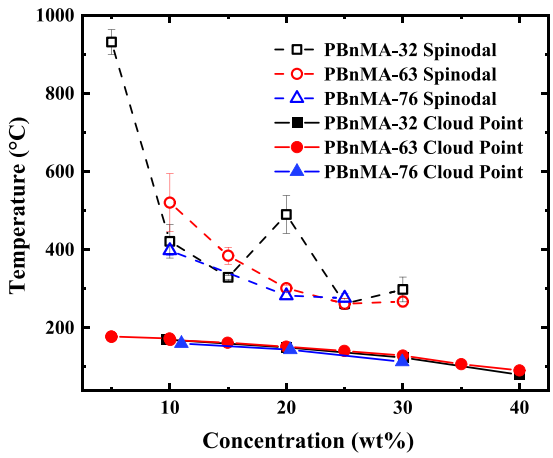

Figure 4. Phase diagram for PBnMA in [BMP][TFSI] with spinodal temperatures (open symbols) and cloud point temperatures (filled symbols) as previously reported.[11] The lines serve as the guide to the eye.

from 25 °C to their respective phase separation temperatures. Additionally, the concentration dependence of ξ was examined, and representative double logarithmic plots of the correlation length of PBnMA as a function of concentration at 25 and 150 °C are shown in Figure 5a,b for [BMP][TFSI] at various temperatures and for various ILs at 25 °C, respectively. The correlation length decreases as the concentration of PBnMA increases, up to 0.3 g/mL, where it either levels off or increases slightly. Whereas ξ is independent of molecular weight, it increases with decreasing solvent quality, which is achieved by increasing the solution temperature (observable in Figure 5a) or varying the cation identity (Figure 5b). The apparent power-law concentration scaling ($\xi \propto c^e$, where e is the scaling exponent) at low concentrations (<0.3 g/mL) is the concentration regime in which solutions are semidilute. This concentration dependence of ξ weakens as the solvent quality decreases and is readily observed between different temperatures in [BMP][TFSI]; however, the difference is much smaller when varying the cation identity at 25 °C.

Upon normalizing the correlation length to the hydrodynamic radius at infinite dilution (ξ/R_h) and the concentration to an approximant of the overlap concentration ($c/[3M/(4\pi R_h^3 N_A)]$), the semidilute correlation lengths of PBnMA in [BMP][TFSI] at various temperatures collapse onto a master curve, as shown in Figure 6a. However, a universal curve among the four ILs was not observed upon similar normalization at 25 °C (Figure 6b). The hydrodynamic radius at infinite dilution (R_h) was calculated by $R_h = bM_w^{\nu}$, where ν and b are the Flory exponent and prefactor, respectively, as measured in previous studies by Kharel et al. and assuming that the exponent is independent of temperature.[10] At low concentrations or high temperatures, the correlation length is large and exhibits weak concentration dependence, whereas at high normalized concentrations or low temperatures, the correlation length is small but exhibits strong concentration dependence.

The normalized semidilute correlation length of PBnMA in an IL at any individual temperature follows an approximate power-law scaling exponent. Lines of best fit to the data in Figure 6a are shown in Figure S27. The resulting scaling exponents ($\xi/R_h \propto c^e$) of PBnMA in [BMP][TFSI] as a function of solution temperature are collected in Figure 7a. A

https://doi.org/10.1021/acs.macromol.2c01365
Macromolecules XXXX, XXX, XXX−XXX

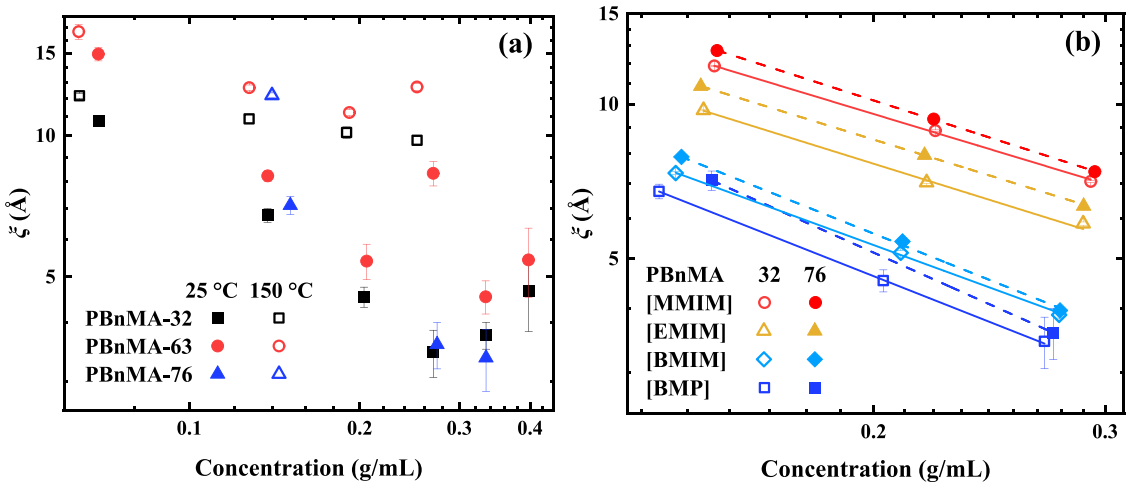

Figure 5. Double-logarithmic plot of ξ vs concentration for PBnMA in (a) [BMP][TFSI] at 25 °C (open symbols) and 150 °C (filled symbols) and in (b) various ILs at 25 °C for several molecular weights. The lines of best fit represent the power-law concentration scaling following the form $\xi \propto c^e$.

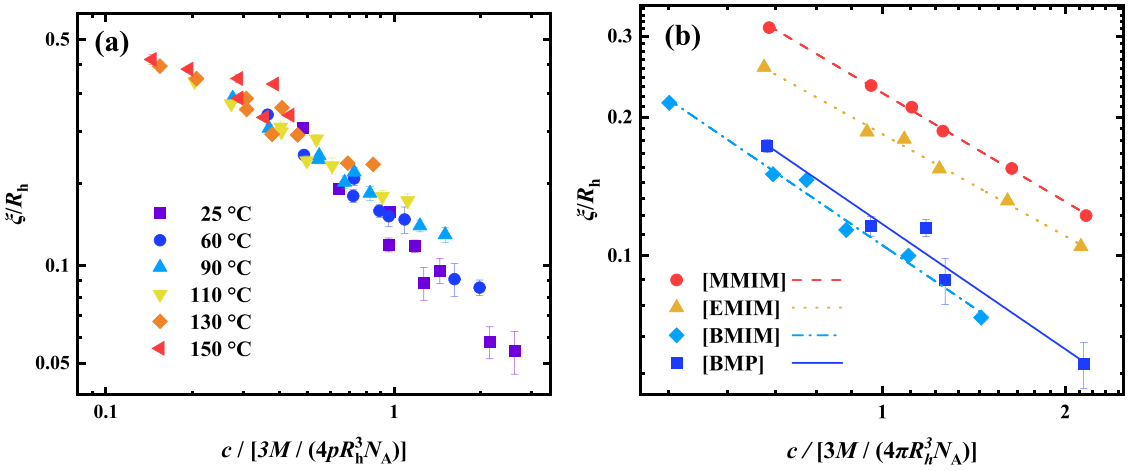

Figure 6. Double logarithmic curves of the normalized correlation length vs normalized concentration for semidilute (a) PBnMA-32, PBnMA-63, and PBnMA-76 in [BMP][TFSI] at various temperatures and for (b) PBnMA-32 and PBnMA-76 in various ILs at 25 °C. The lines of best fit represent the power-law concentration scaling following the form $\xi \propto c^e$.

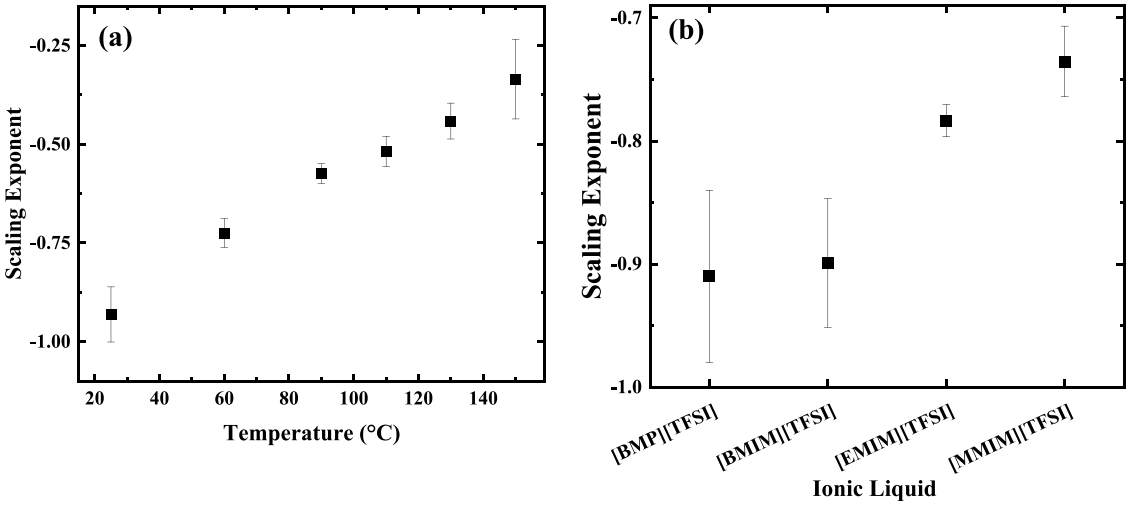

Figure 7. Solvent quality dependence of the apparent semidilute correlation length concentration-scaling exponent, e, of the form $\xi \propto c^e$ for PBnMA in (a) [BMP][TFSI] at various temperatures and in (b) various ILs at 25 °C.

https://doi.org/10.1021/acs.macromol.2c01365
Macromolecules XXXX, XXX, XXX−XXX

monotonic increase in the scaling exponent from −0.91 ± 0.07 to −0.4 ± 0.1 is observed as the solutions are heated from 25 to 150 °C. Similarly, the scaling exponents at 25 °C are shown to increase as the solvent quality worsens by varying the cation identity from [BMP] to [MMIM], yielding exponents ranging from −0.91 ± 0.07 to −0.74 ± 0.03, as shown in Figure 7b.

■ DISCUSSION

Lower critical solution temperature phase behavior in polymer/IL solutions can arise from strong interactions between the polymeric solute and the solvent. In the context of Flory−Huggins theory, this can be attributed to a positive excess entropic contribution (A) and a negative enthalpic contribution (B) to χ ($\chi = A + B/T$). Previous simulations for PBnMA in [EMIM][TFSI] by Fujii et al. revealed that PBnMA preferentially interacts with either the cation or adjacent benzyl groups rather than with the TFSI anion.[9] Thus, the entropic contribution to χ is positive for PBnMA in ILs primarily due to the cation-π solvation clathrate between the cation and the aromatic ring in the benzyl methacrylate repeat unit.[27] This attraction also gives rise to the negative value of B. The observed increase in the magnitudes of A and B with concentration indicates the entropic penalty and enthalpic benefit for mixing increases beyond the contribution anticipated by the $\phi(1 - \phi)\chi$ term in Flory−Huggins theory. This has been observed for a similar polymer/IL system, poly(n-butyl methacrylate) in mixtures of [BMIM][TFSI] and [EMIM][TFSI], where Hoarfrost et al. proposed that the solvation structure of ILs around the nonpolar n-butyl groups directly influences the excess entropy and enthalpy of mixing.[28] In an analogous manner, the excess entropy of mixing for PBnMA in [BMP][TFSI] may increase with concentration because of the loss of translational freedom for the IL as more cations are bound within the solvation clathrate and the increase in the enthalpy of mixing may arise from the greater number of polymer−solvent interactions.

One of the fundamental assumptions of Flory−Huggins theory is that χ is independent of concentration; this has been confirmed for a variety of systems such as polystyrene in tetrahydrofuran and polyethylene/poly(ethylene propylene) blends.[19,29,30] However, a concentration-dependent χ has also been observed in numerous polymer blends and solutions, including polystyrene/poly(vinyl methyl ether) blends and poly(dimethyl siloxane) in methylethylketone.[13,18] For PBnMA in ILs, the overall increase in χ with concentration is a result of the entropic penalty of mixing overcoming the enthalpic benefit at higher compositions. A similar concentration dependence has been observed in solutions without strong solute−solvent interactions (e.g., polystyrene in cyclohexane), and as such, it is uncertain whether the concentration dependence of χ, A, and B are solely a result of IL solvation.[31] Alternative arguments have been proposed based upon cohesive energy density differences, chain-end effects, component size asymmetry, chain stiffness, and free volume differences; however, the precise origin of this compositional dependence is not known and may vary from system to system.[13,31−36] Nevertheless, the results indicate that χ determined via light scattering in dilute solutions is not always a reliable guide for higher compositions, as evidenced by the previous unusual observation that the second virial coefficient of dilute PBnMA/IL solutions is consistently positive even at temperatures above phase separation for higher concentrations.[10]

Previous work characterizing the cloud point temperatures of PBnMA in [BMP][TFSI] demonstrated that the critical compositions of these systems are shifted substantially toward polymer-rich compositions, in contrast to the solvent-rich compositions anticipated by Flory−Huggins theory.[11] Similarly, the spinodal temperatures in Figure 4 decrease throughout the entire composition window under study, further confirming that the critical composition is indeed shifted. This deviation is also reinforced by the large temperature window between the spinodal and binodal curves at 30 wt % (*ca.* 150 °C), as these curves should converge in the vicinity of the critical point. This phenomenon can be rationalized as a consequence of χ increasing with concentration as hypothesized by Schäfer-Soenen and co-workers, thereby decreasing the miscibility of the polymer in the ionic liquid and lowering the phase separation temperatures.[37]

An additional argument has been proposed by White and Lipson to rationalize the unusual phase diagram of poly(ethylene oxide) in 1-ethyl-3-methylimidazolium tetrafluoroborate ([EMIM][BF_4]), which exhibits critical compositions ranging from 50 to 80 wt % polymer.[38−40] They postulate that local ordering of the IL reduces the entropy of mixing, and the large IL cohesive energy density shifts the critical composition to polymer-rich concentrations. This may be supported by the presence of low-q peaks in wide-angle X-ray scattering patterns of the pure ILs and polymer/IL solutions (Figure S28), which indicate local ordering of the IL is maintained even in the presence of PBnMA.[41,42] In an analogous manner, the appearance of a small broad peak at high-q in the pure-IL SAXS patterns (Figure S8) further suggests local ordering of the IL.[26] However, there are several polymer/IL systems in which the IL shows such spatial correlations, such as poly(ethyl glycidyl ether) in 1-alkyl-3-methylimidazolium bis(trifluoromethyl-sulfonyl)imide or poly(n-butyl methacrylate) in [BMIM][TFSI], yet the critical compositions are still found at dilute concentrations.[28,43,44] Thus, there remains uncertainty surrounding the origin of the polymer-rich critical composition. In contrast, the molecular weight independence of the cloud point and spinodal temperatures is an interesting, yet anticipated, characteristic in LCST systems. The large entropic penalty ($A > 0.5$) and enthalpic benefit ($B < 0$) upon mixing − which gives rise to LCST behavior − results in this independence for high molecular weight chains and has been previously observed for poly(ethylene oxide) in 1-ethyl-3-methylimidazolium tetrafluoroborate and for PBnMA in [BMP][TFSI].[11,25,40]

The correlation length (ξ) for a polymer solution reflects the distance over which intrachain excluded volume interactions are screened. At distances smaller than ξ, different chains do not interact but behave similarly to isolated chains in dilute solutions. At distances beyond ξ, chains interact with adjacent segments in solution which counteracts the excluded volume effects due to the solvent.[12] ξ is shown to increase with decreasing solvent quality, both in the case of increasing temperature and when varying the IL cation identity. This suggests concentration fluctuations grow in intensity as solutions lie closer to the phase boundary, an inference further supported by the weaker temperature dependence of ξ in [BMP][TFSI] at low concentrations, which lie farther from both the spinodal curve and critical composition.

For semidilute solutions, ξ is anticipated to decrease with concentration according to power-law decay.[19] The ξ of PBnMA in [BMP][TFSI] exhibits an apparent power-law

https://doi.org/10.1021/acs.macromol.2c01365
Macromolecules XXXX, XXX, XXX−XXX

scaling between concentrations of 0.07 to 0.3 g/mL, but then either levels off or increases slightly (see Figures 5 and S24). A similar concentration boundary beyond the semidilute regime has been seen for polystyrene in toluene.[45] Nevertheless, the correlation length for any molecular weight should collapse onto a universal curve as a function of concentration.[19,46] However, it has not yet been seen that the position along the master curve can be further tuned through changing the temperature, or correspondingly, the solvent quality according to a concentration−temperature superposition, as can be seen in Figure 6a for PBnMA in [BMP][TFSI]. This indicates that chains behave in a similar manner, regardless of temperature, polymer molecular weight, or solution concentration. However, this master curve is not universal across all four ILs; thus, there are additional system-dependent factors that influence the correlation length.

The blob model predicts that the correlation length follows a power-law concentration scaling of the form $\xi \propto c^e$, where e increases from −3/4 for a good solvent to −1 for a theta solvent.[12,19,47−49] This scaling has been verified for several systems, with exponents of −0.80 ± 0.03 for poly(methyl methacrylate) in chloroform at 25 °C, −0.76 for hydrogenated poly(butadiene) in $C_{16}D_{34}$ at 140 °C, and −0.70 ± 0.02 for poly(styrene) in toluene.[50−52] In contrast, the scaling exponent for PBnMA in [BMP][TFSI] exhibits a monotonic increase from −0.91 ± 0.07 to −0.4 ± 0.1 as the solutions are heated from 25 °C (good solvent) to 150 °C (near phase separation). Analogously, the scaling exponent at 25 °C increased to −0.4 ± 0.1 as the IL was varied from [BMP][TFSI] to [MMIM][TFSI], in order of decreased solvent quality. Similar deviations have been reported in previous light scattering experiments of polystyrene in *trans*-decalin by Chu and Nose, who reported scaling exponents of −0.63 ± 0.01 and −0.61 ± 0.01 at 40 and 30 °C, respectively.[53] They posited that this deviation occurs because the polymer solutions are in a transition region between a theta solvent (T_Θ = 20.5 °C) and good solvent. This disagreement was also seen for polystyrene in cyclohexane, which exhibits a scaling exponent of −0.65 according to SAXS measurements by Kinugasa et al.[54] In both cases, the magnitude of the observed scaling exponent is lower than anticipated for either a good or theta solvent according to the blob model, similar to the trend exhibited in this study. The origin of this behavior is also as yet unresolved.

■ CONCLUSIONS

In this work, we assessed the interaction parameter and correlation length of semidilute PBnMA/IL solutions exhibiting LCST phase behavior over wide ranges of concentration, temperature, and molecular weight via SAXS. In contrast to the classical Flory−Huggins theory, χ values determined from RPA analysis were shown to increase with polymer volume fraction, resulting in a shift of the critical concentration to polymer-rich compositions. This shift was also reflected in the experimental spinodal curves of PBnMA in [BMP][TFSI], determined from Ornstein−Zernike analysis. Consistent with previous solvent quality studies, the interaction parameter increases by increasing the temperature in an LCST system, varying the imidazolium-cation alkyl chain length from methyl to butyl and changing the cation identity to pyrrolidinium. In semidilute [BMP][TFSI] solutions, the correlation length was shown to obey a concentration−temperature superposition when normalized against the hydrodynamic radius at infinite dilution; however, no universal behavior was observed among all four ILs. Additionally, ξ was shown to exhibit power-law concentration scaling exponents which increased as the solvent quality worsened, achieved by increasing the temperature of [BMP][TFSI] solutions or varying the cation identity, in contrast to the blob model values of −3/4 for a good solvent and −1 for a theta solvent. While these results help to rationalize the unusual LCST phase behavior of polymers in ionic liquids, they also pose additional fundamental questions surrounding the statistical behavior of highly interacting systems in semidilute solutions.

■ ASSOCIATED CONTENT

Supporting Information

The Supporting Information is available free of charge at https://pubs.acs.org/doi/10.1021/acs.macromol.2c01365.

SEC traces for all polymers; NMR spectra for polymers and ionic liquids; temperature dependence of viscosity for selected solutions; SAXS profiles for ionic liquids and all solutions; Ornstein−Zernike plots for all solutions; temperature and concentration dependence of interaction parameters; temperature and concentration dependence of the correlation length; and WAXS profiles of selected ionic liquids and solutions (PDF)

■ AUTHOR INFORMATION

Corresponding Author

Timothy P. Lodge − *Department of Chemistry and Department of Chemical Engineering and Materials Science, University of Minnesota, Minneapolis, Minnesota 55455, United States*; orcid.org/0000-0001-5916-8834; Email: lodge@umn.edu

Authors

Brian R. Carrick − *Department of Chemistry and Department of Chemical Engineering and Materials Science, University of Minnesota, Minneapolis, Minnesota 55455, United States*

Steven Weigand − *Argonne National Laboratory, Lemont, Illinois 60439, United States*

Claire L. Seitzinger − *Department of Chemistry, University of Minnesota, Minneapolis, Minnesota 55455, United States*; orcid.org/0000-0002-4700-9964

Complete contact information is available at: https://pubs.acs.org/10.1021/acs.macromol.2c01365

Notes

The authors declare no competing financial interest.

■ ACKNOWLEDGMENTS

This work was supported by the National Science Foundation (Award DMR-2103630), the University of Minnesota Office of Undergraduate Research, and a University of Minnesota Department of Chemistry Summer Research Fellowship. We are grateful to Dr. Cecilia Hall for the synthesis of PBnMA-63, and helpful discussions with Dr. David Giles are appreciated. Portions of this work were performed at the 5-ID-D beamline of the Dupont-Northwestern-Dow Access Team (DND-CAT) at the Advanced Photon Source, Argonne National Laboratory, as well as within the Characterization Facility, College of Science and Engineering, University of Minnesota, which receives partial support from the NSF through the MRSEC (Award Number DMR-2011401) and the NNCI (Award Number ECCS-2025124) programs.

REFERENCES

(1) Bai, J.; Lu, H.; Cao, Y.; Li, X.; Wang, J. A Novel Ionic Liquid Polymer Electrolyte for Quasi-Solid State Lithium Air Batteries. *RSC Adv.* **2017**, *7*, 30603−30609.

(2) Gu, Y.; Cussler, E. L.; Lodge, T. P. ABA-Triblock Copolymer Ion Gels for CO2 Separation Applications. *J. Membr. Sci.* **2012**, *423*−*424*, 20−26.

(3) Tang, B.; Schneiderman, D. K.; Zare Bidoky, F.; Frisbie, C. D.; Lodge, T. P. Printable, Degradable, and Biocompatible Ion Gels from a Renewable ABA Triblock Polyester and a Low Toxicity Ionic Liquid. *ACS Macro Lett.* **2017**, *6*, 1083−1088.

(4) Choi, J. H.; Xie, W.; Gu, Y.; Frisbie, C. D.; Lodge, T. P. Single Ion Conducting, Polymerized Ionic Liquid Triblock Copolymer Films: High Capacitance Electrolyte Gates for n-Type Transistors. *ACS Appl. Mater. Interfaces* **2015**, *7*, 7294−7302.

(5) Lodge, T. P. A Unique Platform for Materials Design. *Science* **2008**, *321*, 50−51.

(6) Watanabe, M. Advances in Organic Ionic Materials Based on Ionic Liquids and Polymers. *Bull. Chem. Soc. Jpn.* **2021**, *94*, 2739−2769.

(7) Ueki, T.; Watanabe, M. Lower Critical Solution Temperature Behavior of Linear Polymers in Ionic Liquids and the Corresponding Volume Phase Transition of Polymer Gels. *Langmuir* **2007**, *23*, 988−990.

(8) Fujii, K.; Ueki, T.; Niitsuma, K.; Matsunaga, T.; Watanabe, M.; Shibayama, M. Structural Aspects of the LCST Phase Behavior of Poly(Benzyl Methacrylate) in Room-Temperature Ionic Liquid. *Polymer* **2011**, *52*, 1589−1595.

(9) Fujii, K.; Ueki, T.; Hashimoto, K.; Kobayashi, Y.; Kitazawa, Y.; Hirosawa, K.; Matsugami, M.; Ohara, K.; Watanabe, M.; Shibayama, M. Microscopic Structure of Solvated Poly(Benzyl Methacrylate) in an Imidazolium-Based Ionic Liquid: High-Energy X-Ray Total Scattering and All-Atom MD Simulation Study. *Macromolecules* **2017**, *50*, 4780−4786.

(10) Kharel, A.; Hall, C.; Ernoch, P.; Stepanek, P.; Lodge, T. P. Dilute Solution Properties of Poly(Benzyl Methacrylate) in Ionic Liquids. *Macromolecules* **2020**, *53*, 885−894.

(11) Carrick, B. R.; Seitzinger, C. L.; Lodge, T. P. Unusual Lower Critical Solution Temperature Phase Behavior of Poly(Benzyl Methacrylate) in a Pyrrolidinium-Based Ionic Liquid. *Molecules* **2021**, *26*, 4850.

(12) de Gennes, P. G. *Scaling Concepts in Polymer Physics*; Cornell University Press: London, 1979.

(13) Muramoto, A. Dependence of Interaction Parameter on Molecular Weight and Concentration for Solutions of Poly-(Dimethylsiloxane) in Methylethylketone. *Polymer* **1982**, *23*, 1311−1316.

(14) Aoki, Y.; Wang, H.; Sharratt, W.; Dalgliesh, R. M.; Higgins, J. S.; Cabral, T. Small Angle Neutron Scattering Study of the Thermodynamics of Highly Interacting PαMSAN/DPMMA Blends. *Macromolecules* **2019**, *52*, 1112−1124.

(15) Aoki, Y.; Sharratt, W.; Wang, H.; O'Connell, R.; Pellegrino, L.; Rogers, S.; Dalgliesh, R. M.; Higgins, J. S.; Cabral, J. T. Effect of Tacticity on the Phase Behavior and Demixing of PαMSAN/DPMMA Blends Investigated by SANS. *Macromolecules* **2020**, *53*, 445−457.

(16) O'Connell, R. A.; Sharratt, W. N.; Aelmans, N. J. J.; Higgins, J. S.; Cabral, J. T. SANS Study of PPPO in Mixed Solvents and Impact on Polymer Nanoprecipitation. *Macromolecules* **2022**, *55*, 1050−1059.

(17) Bates, F. S.; Koehler, W. C.; Wignall, G. D.; Fetters, L. J. SANS Evaluation of the RPA Theory for Binary Homopolymer Mixtures. *Symposium on Scattering from Block Copolymers and Model Systems*: Boston, MA, Dec 1, 1986.

(18) Han, C. C.; Bauer, B. J.; Clark, J. C.; Muroga, Y.; Matsushita, Y.; Okada, M.; Tran-cong, Q.; Chang, T.; Sanchez, I. C. Temperature, Composition and Molecular-Weight Dependence of the Binary Interaction Parameter of Polystyrene/Poly(Vinyl Methyl Ether) Blends. *Polymer* **1988**, *29*, 2002−2014.

(19) Graessley, W. W. *Polymeric Liquids & Networks: Structure and Properties*; Garland Science, Taylor & Francis Group: New York, 2004.

(20) Podzimek, S. *Light Scattering, Size Exclusion Chromatography and Asymmetric Flow Field Flow Fractionation: Powerful Tools for the Characterization of Polymers*; John Wiley & Sons: New Jersey, 2011.

(21) Seitzinger, C. L.; Hall, C. C.; Lodge, T. P. Photoreversible Order−Disorder Transitions in Block Copolymer/Ionic Liquid Solutions. *Macromolecules* **2022**, *55*, 3811−3820.

(22) Tokuda, H.; Ishii, K.; Abu Bin, M.; Susan, H.; Tsuzuki, S.; Hayamizu, K.; Watanabe, M. Physicochemical Properties and Structures of Room-Temperature Ionic Liquids. 3. Variation of Cationic Structures. *J. Phys. Chem. B* **2006**, *110*, 2833−2839.

(23) Mandal, T. K.; Kuo, J. F.; Woo, E. M. Miscibility and Spherulite Growth Kinetics in the Poly(Ethylene Oxide)/Poly(Benzyl Methacrylate) System. *J. Polym. Sci., Part B: Polym. Phys.* **2000**, *38*, 562−572.

(24) Tokuda, H.; Hayamizu, K.; Ishii, K.; Abu Bin Hasan Susan, M.; Watanabe, M. Physicochemical Properties and Structures of Room Temperature Ionic Liquids. 2. Variation of Alkyl Chain Length in Imidazolium Cation. *J. Phys. Chem. B* **2005**, *109*, 6103−6110.

(25) Lodge, T. P.; Hiemenz, P. C. *Polymer Chemistry*, 3rd ed.; CRC Press: Boca Raton, 2020.

(26) Wong, L. N.; Jones, S. D.; Wood, K.; De Campo, L.; Darwish, T.; Moir, M.; Li, H.; Segalman, R. A.; Warr, G. G.; Atkin, R. Polycation Radius of Gyration in a Polymeric Ionic Liquid (PIL): The PIL Melt Is Not a Theta Solvent. *Phys. Chem. Chem. Phys.* **2022**, *24*, 4526−4532.

(27) Ueki, T.; Arai, A. A.; Kodama, K.; Kaino, S.; Takada, N.; Morita, T.; Nishikawa, K.; Watanabe, M. Thermodynamic Study of Phase Transitions of Poly(Benzyl Methacrylate) in Ionic Liquid Solvents. *Pure Appl. Chem.* **2009**, *81*, 1829−1841.

(28) Hoarfrost, M. L.; He, Y.; Lodge, T. P. Lower Critical Solution Temperature Phase Behavior of Poly(n-Butyl Methacrylate) in Ionic Liquid Mixtures. *Macromolecules* **2013**, *46*, 9464−9472.

(29) Maurer, W. W.; Bates, F. S.; Lodge, T. P.; Almdal, K.; Mortensen, K.; Fredrickson, G. H. Can a Single Function for χ Account for Block Copolymer and Homopolymer Blend Phase Behavior? *J. Chem. Phys.* **1998**, *108*, 2989.

(30) Brown, W.; Mortensen, K. Comparison of Correlation Lengths in Semidilute Polystyrene Solutions in Good Solvents by Quasi-Elastic Light Scattering and Small-Angle Neutron Scattering. *Macromolecules* **1988**, *21*, 420−425.

(31) Krigbaum, W. R.; Geymer, D. O. Thermodynamics of Polymer Solutions. The Polystyrene-Cyclohexane System near the Flory Theta Temperature. *J. Am. Chem. Soc.* **1959**, *81*, 1859−1868.

(32) Muthukumar, M. Thermodynamics of Polymer Solutions. *J. Chem. Phys.* **1986**, *85*, 4722.

(33) Muthukumar, M.; Edwards, S. F. Extrapolation Formulas for Polymer Solution Properties. *J. Chem. Phys.* **1982**, *76*, 2720.

(34) Sanchez, I. C. Volume Fluctuation Thermodynamics of Polymer Solutions. *Macromolecules* **1991**, *24*, 908−916.

(35) Koningsveld, R.; Kleintjens, L. A.; Schoffeleers, H. M. Thermodynamic Aspects of Polymer Compatibility. *Pure Appl. Chem.* **1974**, *39*, 1−32.

(36) Fredrickson, G. H.; Liu, A. J.; Bates, F. S. Entropic Corrections to the Flory-Huggins Theory of Polymer Blends: Architectural and Conformational Effects. *Macromolecules* **1994**, *27*, 2503−2511.

(37) Schäfer-Soenen, H.; Moerkerke, R.; Berghmans, H.; Koningsveld, R.; Dušek, K.; Šolc, K. Zero and Off-Zero Critical Concentrations in Systems Containing Polydisperse Polymers with Very High Molar Masses. 2. The System Water-Poly(Vinyl Methyl Ether). *Macromolecules* **1997**, *30*, 410−416.

(38) White, R. P.; Lipson, J. E. G. Origins of Unusual Phase Behavior in Polymer/Ionic Liquid Solutions. *Macromolecules* **2013**, *46*, 5714−5723.

(39) Lee, H. N.; Lodge, T. P. Lower Critical Solution Temperature (LCST) Phase Behavior of Poly(Ethylene Oxide) in Ionic Liquids. *J. Phys. Chem. Lett.* **2010**, *1*, 1962−1966.

https://doi.org/10.1021/acs.macromol.2c01365
Macromolecules XXXX, XXX, XXX−XXX

(40) Lee, H. N.; Newell, N.; Bai, Z.; Lodge, T. P. Unusual Lower Critical Solution Temperature Phase Behavior of Poly(Ethylene Oxide) in Ionic Liquids. *Macromolecules* **2012**, *45*, 3627−3633.
(41) Hayes, R.; Warr, G. G.; Atkin, R. Structure and Nanostructure in Ionic Liquids. *Chem. Rev.* **2015**, *115*, 6357−6426.
(42) Santos, C. S.; Murthy, N. S.; Baker, G. A.; Castner, E. W., Jr. Communication: X-Ray Scattering from Ionic Liquids with Pyrrolidinium Cations. *J. Chem. Phys.* **2011**, *134*, 121101.
(43) Tsuda, R.; Kodama, K.; Ueki, T.; Kokubo, H.; Imabayashi, S. I.; Watanabe, M. LCST-Type Liquid-Liquid Phase Separation Behaviour of Poly(Ethylene Oxide) Derivatives in an Ionic Liquid. *Chem. Commun.* **2008**, *40*, 4939−4941.
(44) Kodama, K.; Tsuda, R.; Niitsuma, K.; Tamura, T.; Ueki, T.; Kokubo, H.; Watanabe, M. Structural Effects of Polyethers and Ionic Liquids in Their Binary Mixtures on Lower Critical Solution Temperature Liquid-Liquid Phase Separation. *Polym. J.* **2011**, *43*, 242−248.
(45) Brown, W.; Mortensen, K.; Floudas, G. Screening Lengths in Concentrated Polystyrene Solutions in Toluene Determined Using Small Angle Neutron and Small Angle X-Ray Scattering. *Macromolecules* **1992**, *25*, 6904−6908.
(46) Hamada, F.; Kinugasa, S.; Hayashi, H.; Nakajima, A. Small-Angle X-Ray Scattering from Semidilute Polymer Solutions 1. Polystyrene in Toluene. *Macromolecules* **1985**, *18*, 2290−2294.
(47) Farnoux, B.; Boue, F.; Cotton, J. P.; Daoud, M.; Jannink, G.; Nierlich, M.; De Gennes, P. G. Cross-over in Polymer Solutions. *J. Phys.* **1978**, *39*, 77−86.
(48) Cotton, J. P.; Nierlich, M.; Boue, F.; Daoud, M.; Farnoux, B.; Jannink, G.; Duplessix, R.; Picot, C. Experimental Determination of the Temperature-Concentration Diagram of Flexible Polymer Solutions by Neutron Scattering. *J. Chem. Phys.* **1976**, *65*, 1101−1108.
(49) Daoud, M.; Cotton, J. P.; Farnoux, B.; Jannink, G.; Sarma, G.; Benoit, H.; Duplessix, C.; Picot, C.; de Gennes, P. G. Solutions of Flexible Polymers, Neutron Experiments and Interpretation. *Macromolecules* **1975**, *8*, 804−818.
(50) King, J. S.; Boyer, W.; Wignall, G. D.; Ullman, R. Radii of Gyration and Screening Lengths of Polystyrene in Toluene as a Function of Concentration. *Macromolecules* **1985**, *18*, 709−718.
(51) Tao, H.; Huang, C. I.; Lodge, T. P. Correlation Length and Entanglement Spacing in Concentrated Hydrogenated Polybutadiene Solutions. *Macromolecules* **1999**, *32*, 1212−1217.
(52) Cheng, G.; Graessley, W. W.; Melnichenko, Y. B. Polymer Dimensions in Good Solvents: Crossover from Semidilute to Concentrated Solutions. *Phys. Rev. Lett.* **2009**, *102*, 157801.
(53) Chu, B.; Nose, T. Static and Dynamical Properties of Polystyrene in Trans-Decalin. 4. Osmotic Compressibility, Characteristic Lengths, and Internal and Pseudogel Motions in the Semidilute Regime. *Macromolecules* **1980**, *13*, 122−132.
(54) Kinugasa, S.; Hayashi, H.; Hamada, F.; Nakajima, A. Small-Angle x-Ray Scattering from Semidilute Polymer Solutions. 2. Polystyrene in Cyclohexane. *Macromolecules* **1986**, *19*, 2832−2840.

https://doi.org/10.1021/acs.macromol.2c01365
Macromolecules XXXX, XXX, XXX−XXX